ARMY RESEARCH LABORATORY

Hybrid Fiber Sizings for Enhanced Energy Absorption in Glass-Reinforced Composites

by Robert E. Jensen, Steven H. McKnight, Dave P. Flanagan, Alan R. Teets, and Donovan Harris

ARL-TR-3241 **July 2004**

NOTICES

Disclaimers

The findings in this report are not to be construed as an official Department of the Army position unless so designated by other authorized documents.

Citation of manufacturer's or trade names does not constitute an official endorsement or approval of the use thereof.

Destroy this report when it is no longer needed. Do not return it to the originator.

Army Research Laboratory
Aberdeen Proving Ground, MD 21005-5069

ARL-TR-3241 **July 2004**

Hybrid Fiber Sizings for Enhanced Energy Absorption in Glass-Reinforced Composites

Robert E. Jensen, Steven H. McKnight, Dave P. Flanagan, Alan R. Teets, and Donovan Harris
Weapons and Materials Research Directorate, ARL

REPORT DOCUMENTATION PAGE

Form Approved
OMB No. 0704-0188

1. REPORT DATE *(DD-MM-YYYY)*	2. REPORT TYPE	3. DATES COVERED (From - To)
July 2004	Final	September 1999–December 2003

4. TITLE AND SUBTITLE
Hybrid Fiber Sizings for Enhanced Energy Absorption in Glass-Reinforced Composites

5a. CONTRACT NUMBER

5b. GRANT NUMBER

5c. PROGRAM ELEMENT NUMBER

6. AUTHOR(S)
Robert E. Jensen, Steven H. McKnight, Dave P. Flanagan, Alan R. Teets, and Donovan Harris

5d. PROJECT NUMBER
AH42

5e. TASK NUMBER

5f. WORK UNIT NUMBER

7. PERFORMING ORGANIZATION NAME(S) AND ADDRESS(ES)
U.S. Army Research Laboratory
ATTN: AMSRD-ARL-WM-MA
Aberdeen Proving Ground, MD 21005-5069

8. PERFORMING ORGANIZATION REPORT NUMBER
ARL-TR-3241

9. SPONSORING/MONITORING AGENCY NAME(S) AND ADDRESS(ES)

10. SPONSOR/MONITOR'S ACRONYM(S)

11. SPONSOR/MONITOR'S REPORT NUMBER(S)

12. DISTRIBUTION/AVAILABILITY STATEMENT
Approved for public release; distribution is unlimited.

13. SUPPLEMENTARY NOTES

14. ABSTRACT

Achieving high-impact energy absorption without loss of structural performance in a glass fiber-reinforced composite can be obtained through a "materials by design" approach of the fiber matrix interphase through modification of current commercially formulated silane-based fiber-sizing packages. In this report, we document the structural and impact performance of composites produced using a fiber-sizing package designed to provide strong fiber-matrix bonding at low-impact rates and weak fiber-matrix bonding at high-impact rates. Additionally, enhancement of post-failure behavior at high-impact rates via increased absorption of frictional energy during fiber-matrix pullout was explored through control of the surface roughness and texture of the glass fibers. A unique inorganic-organic hybrid fiber-sizing formulation was successfully applied at a commercial E-glass manufacturing facility to produce rovings as well as woven fabric reinforcements. Composite materials were manufactured using these specialized fabrics, and the preliminary structural and impact energy responses of these materials have been measured.

15. SUBJECT TERMS
fiber sizing, E-glass, S-2 Glass, interphase, composite

16. SECURITY CLASSIFICATION OF:			17. LIMITATION OF ABSTRACT	18. NUMBER OF PAGES	19a. NAME OF RESPONSIBLE PERSON
a. REPORT	b. ABSTRACT	c. THIS PAGE			Robert E. Jensen
UNCLASSIFIED	UNCLASSIFIED	UNCLASSIFIED	UL	46	19b. TELEPHONE NUMBER (*Include area code*) 410-306-1910

Contents

List of Figures

List of Tables

Acknowledgments

This research was supported in part by an appointment to the Research Participation Program at the U.S. Army Research Laboratory (ARL) administered by the Oak Ridge Institute for Science and Education through an interagency agreement between the U.S. Department of Energy and ARL. The authors also wish to thank the ARL Composite Materials Research Center of Excellence contract DAAL01-96-2-0048 and the University of Delaware-Center for Composite Materials for partial funding of this project. University of Delaware students Xiao Gao, Nick Theodorakos, and Steven Koellhoffer are acknowledged for their contributions. The authors also wish to acknowledge the technical assistance provided by Phil Madison, Larry Holmes, Paul Moy, John Brown, Jim Wolbert, and Pete Dehmer.

1. Introduction

The effect of silane coupling agents and silane-based sizings on glass fiber-reinforced composite structural performance and durability has been widely studied (*1–6*). Traditionally, silane coupling agents are used to increase the adhesion of the glass fiber reinforcement to the polymeric matrix and to increase the strength retention of the composite upon exposure to wet conditions (*7*, *8*). Surface treatment of glass fibers is accomplished through hydrolysis and subsequent condensation of organo-functional alkoxy silane coupling agents to the silanol groups on the glass surface. Strength and durability is the result of interpenetration and reaction of the composite matrix resin with reactive organic functional groups of the condensed silane network (*9*). Common silane coupling agents used to increase the structural performance/moisture resistance of glass-reinforced composites incorporate epoxy, amine, or methacryl functional groups as the reactive organic component, depending on the chemistry of the matrix resin (*10*, *11*). For industrial glass fiber manufacturing, the silane coupling agent is applied as one of the constituents in a multicomponent fiber-sizing package formulation during the initial stages of production (*12–14*). The role of the silane and the other constituents found in more complex commercial sizings is being investigated more thoroughly in ongoing research.

The static properties of fiber-reinforced composites are often cited regarding advantages with respect to weight and performance over traditional engineering materials (*15*, *16*). However, it is universally accepted that the dynamic response of composite materials is strain-rate dependent and that the fiber-matrix interphase region is the key factor in determining the impact resistance and damage tolerance of fiber-reinforced composites (*17*, *18*). The bulk of published research findings indicates that the impact response of a fiber-reinforced composite can be tailored toward high energy absorption by engineering weak fiber-matrix interfacial interactions or, conversely, high residual strength after impact can be produced by promoting strong fiber-matrix interfacial interactions (*19*). The effective swing in impact performance of a glass fiber-reinforced composite material between a high or low impact energy absorber is most commonly dictated by the choice of silane coupling agent used in the fiber sizings applied during production (*20–23*). For composite panels containing glass fibers pretreated with a silane coupling agent that provides low levels of adhesion between the fiber and matrix, the impact damage areas are large due to fiber-matrix pullout and delamination mechanisms, yielding high energy absorption. As the fiber-matrix bond strength is increased, the flexural strength and strength after impact of the composite will increase. However, this increase in fiber-matrix bonding results in significant fiber breakage during impact, which mitigates fiber pullout and the associated energy absorption mechanisms. These two aspects of composite response to impact mechanisms are generally in opposition.

The desirable achievement of simultaneous high composite strength and energy absorption levels will likely require optimized silane surface pretreatment formulations, as has been suggested (*19*, *24*). Such optimized silane surface pretreatments would certainly involve mixed organic functionalities of varied reactivity toward the polymeric matrix phase. Adhesive bond strength studies between thermoplastic polymers and metal oxide surfaces have been conducted where the density of reactive "sticker" groups along the main backbone chains and corresponding density of reactive "receptor" groups found on the surface of the substrate have been varied (*25*). In this research, the maximum adhesive strength was achieved through a relatively low number of receptor-sticker group interactions. As the number of receptor-sticker group interactions was further increased, the adhesive bond strength decreased. This result was rationalized by a decrease in interfacial entanglements as longer segments of polymer chain are bound to the substrate surface through the increasing numbers of receptor-sticker group interactions. Similar research has also been performed by studying the bond strength of thermosetting epoxy adhesives to silicon wafers treated with varying degrees of octadecyltrichlorosilane, which interacts weakly with the epoxy adhesive (*26*). This study yielded a comparable result in that the epoxy adhesive required a relatively low density of strong surface interactions with the substrate to exhibit maximum bond strength. Also, the bond strength of the epoxy adhesives to the silicon wafers was found to be temperature dependent, with larger numbers of strong interactions required to maintain high bond strength as the temperature is decreased.

Coupled relationships between time and temperature for polymeric materials give rise to experimentally observed viscoelastic responses (*27*). For the fiber-matrix interphase, viscoelastic response has also been alluded to through high strain rate fiber push-out experiments conducted on single fiber composites (*28*). Therefore, a glass fiber sizing package containing a mixture of matrix-compatible and matrix-incompatible silane coupling agents could be developed to serve as an inherent "viscoelastic switch" at the fiber-matrix interphase. In other words, a careful formulation of matrix-compatible and matrix-incompatible silane coupling agents could potentially yield strong fiber-matrix interactions at low strain rates and weak fiber-matrix interactions at high strain rates.

If a triggered interphase response between strong fiber-matrix interactions at low impact rates and weak fiber-matrix interactions at high rates is plausible, then it would be desirable to take maximum advantage of post-failure frictional energy absorption mechanisms via fiber pull-out. Sol-gel chemistry has been used extensively to form *in situ* nanoscale inorganic phases within traditional thermoplastic and thermosetting organic polymers during polymerization (*29–33*) While the majority of these polymerizations are carried out in solutions of tetraethoxysilane (TEOS) or tetramethoxysilane (TMOS), a variety of alkoxides from higher reactivity metals, including titanium, zirconium, aluminum, and boron can be used to form the inorganic phase (*34*). The influence of reaction conditions, acid or base catalyst concentrations, and inorganic-organic stoichiometry ratios with respect to morphology, domain size, optical properties, and macroscopic structural response has also been studied at length (*35–38*). In

addition to being used as *in situ* polymer reinforcements, sol-gel chemistry has also been widely applied in coatings applications, most notably to increase the scratch resistance of glass (*39–42*). Sol-gel chemistries, in which titanium and zirconium alkoxides are used, have also been applied as primers for treating metal oxide surfaces prior to adhesive bonding (*43–45*). While the research and application of inorganic-organic sol-gel chemistry is extensive, to our knowledge these types of reactions have yet to be applied to glass fiber sizings. Sol-gel-based chemistry could potentially be used to increase the surface roughness of commercially produced glass fibers, thereby increasing the coefficient of friction between the fiber and matrix during the fiber pull-out stages of composite failure.

Achieving optimal structural response with concurrent high energy absorption capability in a glass fiber-reinforced composite may be obtainable through a "materials by design" approach and modification of current commercially formulated silane-based fiber-sizing packages. In this report, we document the structural and impact performance of composites produced using fiber-sizing package designed to provide strong fiber-matrix bonding at low impact rates and weak fiber-matrix bonding at high impact rates. Additionally, enhancement of post-failure behavior at high impact rates via increased absorption of frictional energy during fiber-matrix pull-out was explored through control of the surface roughness and texture of the glass fibers. A unique inorganic-organic hybrid fiber-sizing formulation was successfully applied at a commercial E-glass manufacturing facility to produce rovings as well as woven fabric reinforcements. Composite materials were manufactured using these specialized fabrics and the preliminary structural and impact energy responses of E-glass fiber-reinforced composites have been measured.

2. Experimental

2.1 Fiber-Sizing Packages

A series of sizing packages were evaluated in this study: (1) A "hybrid" fiber-sizing package consisting of a mixture of epoxy compatible and incompatible silane coupling agents along with an inorganic fiber surface roughening agent, (2) an "incompatible" fiber-sizing package containing a silane-coupling agent with no chemical reactivity towards an epoxy based matrix, (3) a "compatible" fiber-sizing package containing a silane-coupling agent that is highly chemically reactive towards an epoxy-based matrix, and (4) a "mixed" fiber-sizing package consisting of the identical ratio of epoxy compatible and incompatible silane coupling agents as found in the "hybrid" fiber-sizing package, but minus the fiber surface roughening agent. The aqueous-based fiber-sizing packages were formulated within concentration ranges conducive for industrial production, generally 5%–10% solids in water, including film formers and surfactants. Successful pilot plant scale-up of selected sizing formulations was completed by Fiber Glass

Industries, Inc. (FGI) of Amsterdam, NY. The laboratory sizing formulations were modified slightly by FGI to incorporate additional lubricants, anti-static electricity agents, and other processing aids. Single-end E-glass rovings were manufactured with a 454-kg/m (225-yd/lb) yield, M filaments (~16-μm diameter), and a roving count of 4000 filaments. The custom-sized rovings were subsequently woven into 0.81-kg/m^2 (24-oz/yd^2) plain weave fabrics. In addition to producing plain weave fabrics with identically sized warp and fill direction rovings, FGI was also able to produce mixed weaves with selected sized rovings in the warp direction (hybrid, mixed, or incompatible) and compatible sized rovings in the fill direction of the woven fabric.

2.2 Fiber Characterization

2.2.1 Field Emission-Scanning Electron Microscopy (FE-SEM)

Preliminary surface morphology characterization of the fiber surfaces was carried out using FE-SEM. All fiber samples were rinsed in acetone to remove nonbound components of the sizing package formulations prior to study. The samples were mounted on 25.4-mm-diameter aluminum stubs, using a conductive carbon adhesive. The samples were examined using a Hitachi S-4700 at 1-KeV, 1-μA emission current, and a numerical aperture setting of 7. The samples were positioned so that the fibers were aligned at right angles to the beam scan direction. The micrographs were taken using the lower secondary electron detector, at a nominal working distance of 12 mm.

2.2.2 Atomic Force Microscopy (AFM)

The surface roughness of the compatible- and hybrid-sized E-glass fibers were measured using a Digital Instruments Dimension 3100 AFM. Prior to AFM analysis, the nonsoluble fractions of the sizing formulations, primarily film former, were removed via solvent extraction in acetone. The roughness was measured across the crown of each fiber at 256 lines resolution and 0.78- to 0.50-Hz sampling rate using the tapping mode.

2.3 Roving Friction and Strength

The goal of this research is to develop a fiber-sizing package that enhances frictional dissipation during impact in fully infused and cured composite panels. However, increased friction during the initial fiber-processing stages at the glass manufacturing and weaving facilities is undesirable, as increased friction leads to fiber breakage and processing difficulties. To verify that the film former, lubricants, and other processing aids of the fiber-sizing package remain effective upon incorporation of the inorganic fiber surface roughening agent, the roving friction and strengths were measured. Roving friction was measured using a custom pull-out fixture designed by the U.S. Army Research Laboratory (ARL) and the University of Delaware-Center for Composite Materials (UD-CCM). This pull-out fixture was basically a rectangular aluminum picture frame that allows a spring loaded adjustable lateral tension force to be applied to a woven

fabric while a single roving is pulled in tension. Typically, the woven fabric is cut to allow extra roving material at the bottom of the sample, which keeps the cross-roving contact area and frictional measurement constant during the test.

The roving pull-out fixture was mounted in an Instron model 4505 electro-mechanical testing system equipped with an 89-kN load cell. The crosshead rate during testing was set to 1.27 mm/min. The lateral cross tension of the pull-out fixture was adjusted to a force of ~445 N. Tensile strength measurements of the warp and fill rovings were also completed using the Instron machine at a crosshead rate of 1.27 mm/min and a gauge length of ~152 mm. Rovings of the E-glass fabric with the hybrid sizing and compatible sizing were pulled in both the warp and fill directions. The roving friction and strength measurements were taken as a gauge of the processing ability of the hybrid fiber-sizing package with direct comparisons to the industrial standard compatible fiber-sizing package.

2.4 Pultruded Rod Composite Fabrication

Nonwoven tow packages of the roving treated with the hybrid and compatible sizing formulations were also received from FGI in addition to the woven E-glass fabric. These tow packages were used to produce unidirectional pultruded composite rods using the methods outlined by Thomason (*46*) and Gorowara (*47*). The composite rods were prepared with a volume fraction of fiber equal to ~0.50. The matrix resin consisted of Applied Poleramic, Inc. SC15 epoxy resin. The resin was mixed in the ratio of 100 parts epoxy resin to 30 parts curing agent. The mixed resin was de-gassed under vacuum at 50 °C until no air bubbles were present. The resin was then poured over the fiber roving tows and infused using a hand roller. The resin infused fiber roving tows were then pulled through a fluoropolymer tube with an inside diameter of 9.53 mm. The fluoropolymer tube was then inserted into a close fitting copper pipe for support and to ensure the trueness of the cured composite rods. The composite rods were cured at 200 °C for 3 hr under slight tension with the use of a hanging weight. To minimize thermal stresses, the composite samples were slowly cooled in the oven until they equilibrated at room temperature.

2.5 Composite Panel Fabrication

Composite panels with approximate dimensions of 500 × 500 × 6.35 mm were fabricated using the vacuum assisted resin transfer molding (VARTM) process (*48*). The woven fabric was stacked using 0–90° fabric lay-ups. Applied Poleramic, Inc. SC15 epoxy resin was used as the matrix phase following the same mix ratios and cure schedule as the composite rods. In addition to preparing composite panels using the E-glass material, S-2 Glass reinforced composite panels were also prepared for comparative purposes. The S-2 Glass was a multi-end roving plain weave with a fabric weight of 0.81 kg/m^2 (24 oz/yd^2). The S-2 Glass roving was composed of 9-μm filaments that were treated with a proprietary fiber-sizing package intended to provide a balance of structural strength and impact performance as the reinforcement of a composite material.

Fiber volume fraction of the cured composite panels was calculated using the rules of mixtures and experimentally measured values of density. The density measurements were undertaken using the ASTM D 792-00 testing standard and minimums of five samples for each data set (*49*). Final volume fractions of glass fiber present in the composite panels were calculated to lie between 0.51 and 0.53 for all samples tested. Void content of the cured composite panels was not determined, but appeared void free by visual inspection.

2.6 Composite Mechanical Testing

2.6.1 Short Beam Shear Testing

The composite rods were sectioned into lengths of 60 mm, and the apparent short beam shear strength was measured using ASTM D 4475-85 (*50*), using a 3-point bending apparatus. Testing was completed with span (*s*) to diameter (*d*) ratios set to 3:1 and 5:1. Minimums of five samples were tested for each fiber sizing condition and *s*:*d* ratio. An Instron model 4505 equipped with an 89-kN load cell was used at a crosshead rate of 1.27 mm/min. Breaking force (*P*) was taken from force-vs.-displacement plots, and the apparent shear strength (*S*) was calculated using the following equation:

$$S = \frac{0.849P}{d^2}. \tag{1}$$

2.6.2 Flexural Strength

Flexural strength was measured on 25.4- × 127-mm composite panel samples using the ASTM D 790-96a testing method (*51*). The test was carried out in the 3-point bending mode configuration. Testing was completed with the span length (*L*) to width (*b*) ratio set to 10:1 and 16:1. Minimums of five samples were tested for each fiber sizing condition and *L*:*b* ratio. An Instron model 4505 equipped with an 89-kN load cell was used at a crosshead rate of 1.27 mm/min. Breaking force (*P*) was taken from load-vs.-displacement plots and the maximum fiber stress (σ_{max}) was calculated using the following equation:

$$\sigma_{max} = \frac{3PL}{2bd^2}, \tag{2}$$

where *d* represents the sample thickness.

2.6.3 Tensile Strength

The tensile properties of the composite samples were determined using the ASTM D 3039/D 3039M-95a testing method (*52*). An Instron model 1125 equipped with an 89-kN load cell was used at a crosshead rate of 2.54 mm/min. Minimums of three samples were tested for the compatible and hybrid fiber-sizing conditions. S-2 Glass treated with a compatible sizing was

also tested for comparative purposes. Average sample widths and thicknesses were 25.4 and 3.5 mm, respectively. Breaking forces (P) were taken from force-vs.-displacement plots, and the ultimate tensile strength (F^{tu}) was calculated using the following equation:

$$F^{tu} = \frac{P}{bd}. \tag{3}$$

2.7 Drop Tower Impact Testing

The impact properties of the composite rods were measured using a Dynatup Drop Weight System. The identical 3-point bend fixture as used for the short beam shear strength measurements was used for the impact testing with the s:d ratio set to 3:1. Experimentally measured values of impact energy (E_{impact}), impact velocity (V_{impact}), and maximum force (P_{max}) were recorded from the instrument and are summarized in the results section. The impact energy absorbed to maximum force (E_{max}) and total energy absorbed (E_{total}) were calculated using the instrument software (*53*). Minimums of five samples were tested for each composite rod set.

The impact properties of the composite panels were also measured using the Dynatup Drop Weight System. Samples were cut into 100- × 100-mm squares and impacted with a 12.7-mm-diameter hemispherical indenter. As with the composite rods, the relevant input energies, velocities, and peak loads are summarized in the results section. Absorbed energies were also calculated using the instrument software package (*53*). To measure the post-impact damage area, the damage zone was first visually observed using a light box and outlined with a black permanent marker pen. A digital image was then taken of each damaged panel and a pixel area ratio of the damaged area to undamaged area was analyzed using an image analysis software package (*54*). Actual damage area could then be determined by simply multiplying the actual sample dimensions by the computer-generated pixel ratio. Composite panels were impact tested in as-received condition and after submersion in water at 70 °C for 30 days. Minimums of four samples were tested for each composite panel set.

2.8 Compression After Impact (CAI) Strength

The CAI properties of the composite panels were measured using Suppliers of Advanced Composite Materials Association (SACMA)-recommended method SRM 2R-94 (*55*). Impact damage was generated using the Dynatup Drop Weight System. Samples were cut into 150- × 100-mm rectangles and impacted with a 15.9-mm-diameter hemispherical indenter. The mass of the impacter was adjusted to provide an impact energy of 42.6 J, which closely approximates the energy level of 6.7 J/mm of composite thickness as specified in the standard. Once damaged, the residual compressive strengths of the samples were measured using an Instron model 1332 servo-hydraulic machine equipped with a 222.4-kN load cell. A Boeing CAI

loading test fixture (Wyoming Test Fixtures, Inc.) was used at a crosshead rate of 2.54 mm/min. Ultimate compressive strength (σ_{ult}) was calculated using the following expression:

$$\sigma_{ult} = \frac{P}{bd}. \quad (4)$$

3. Results

3.1 Fiber Characterization: Surface Morphology – Hybrid vs. Compatible Fiber-Sizing Packages

3.1.1 SEM Analysis

A low-magnification SEM image of compatible-sized fiber is shown in figure 1. This SEM image reveals a mostly smooth fiber surface morphology, with the exception of a few defect sites in the glass.

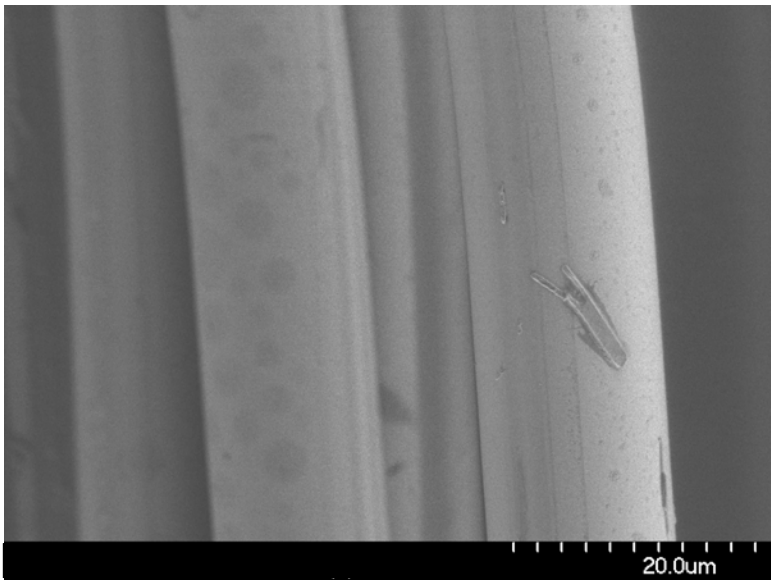

Figure 1. SEM image of E-glass fiber surface treated with compatible sizing after acetone rinse.

A corresponding low-magnification SEM image of the hybrid sized fiber is shown in figure 2. This SEM image displays heterogeneous deposition of the inorganic fiber surface-modifying agent onto the surfaces of the fibers.

SEM characterization of hybrid fiber sizing provides no indication of covalent bonding of inorganic surface-modifying agent to glass fiber surface, although fibers were rinsed in solvent. Some percentage of the inorganic fiber surface-modifying agent present in the hybrid fiber-sizing package may have been washed from the fiber surfaces during the solvent rinse.

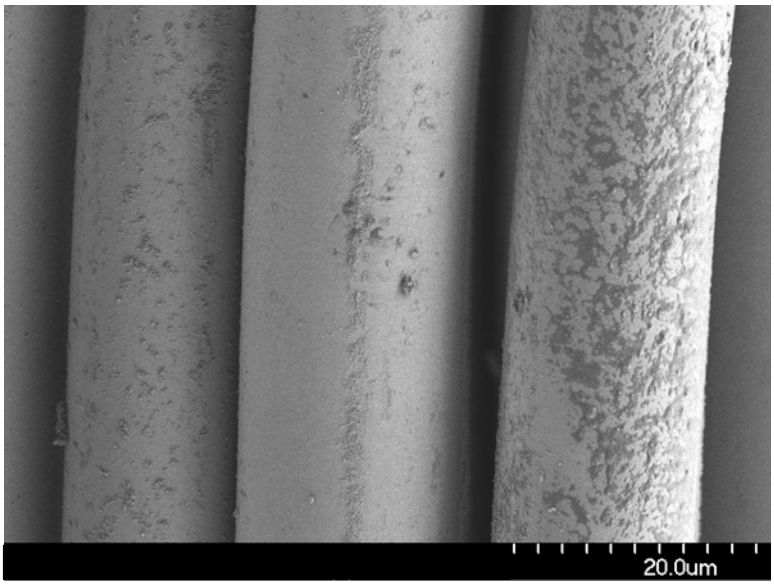

Figure 2. SEM image of E-glass fiber surface treated with hybrid sizing after acetone rinse.

A high-magnification SEM image of compatible-sized fiber is illustrated in figure 3. This SEM image reveals mostly smooth fiber surface morphology, with the exception of a few defect sites in the glass.

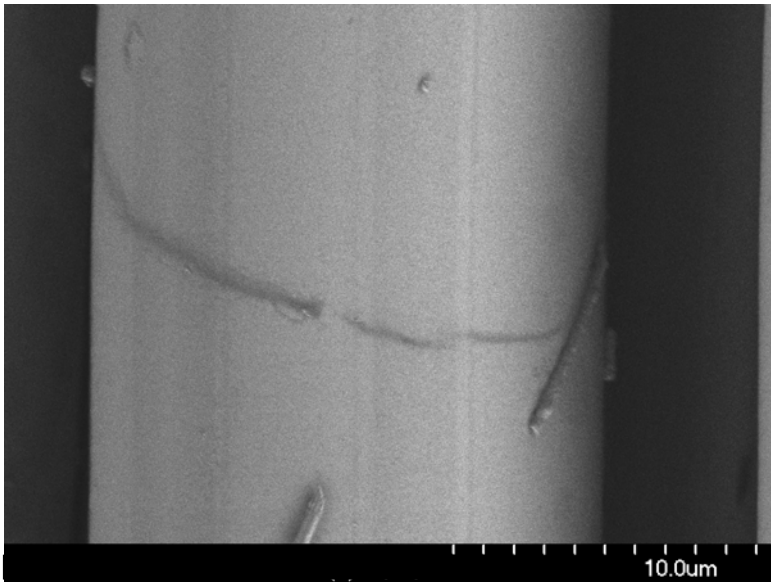

Figure 3. SEM image of E-glass fiber surface treated with compatible sizing after acetone rinse.

A comparative high-magnification SEM image of hybrid-sized fiber is shown in figure 4. This SEM image shows a region of homogeneous dispersion of inorganic surface-modifying agent onto the glass fiber surface. This figure portrays a more "idealized" region envisioned during conceptualization and development of the hybrid fiber-sizing package.

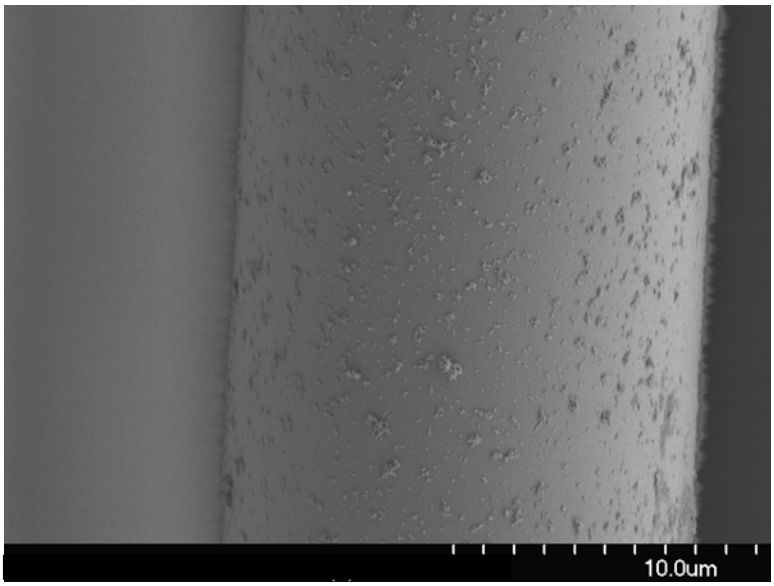

Figure 4. SEM image of E-glass fiber surface treated with hybrid sizing after acetone rinse.

3.1.2 AFM Analysis

The AFM image of the compatible-sized fiber surface is shown in figure 5. The measured RMS roughness was 6.434 nm.

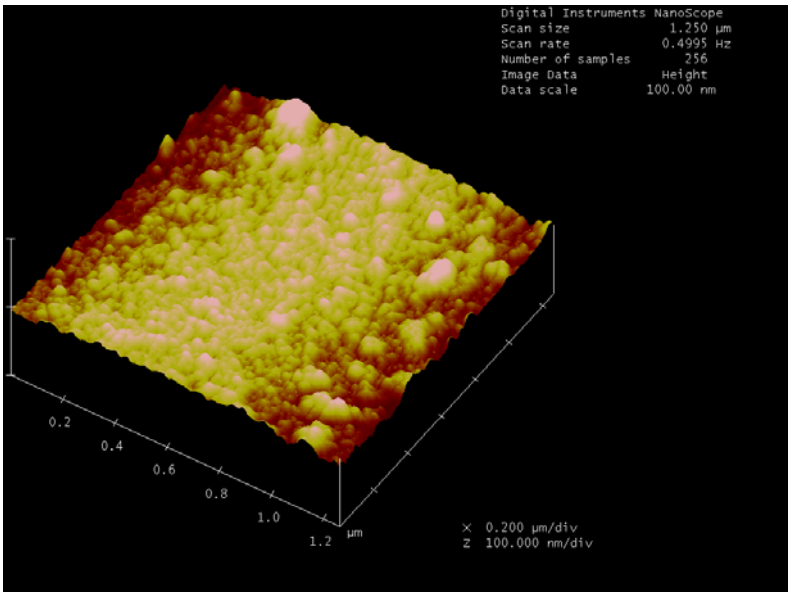

Figure 5. AFM image of compatible-sized E-glass fiber.

The AFM image of the hybrid-sized fiber surface is shown in figure 6. The measured RMS roughness was 37.446 nm.

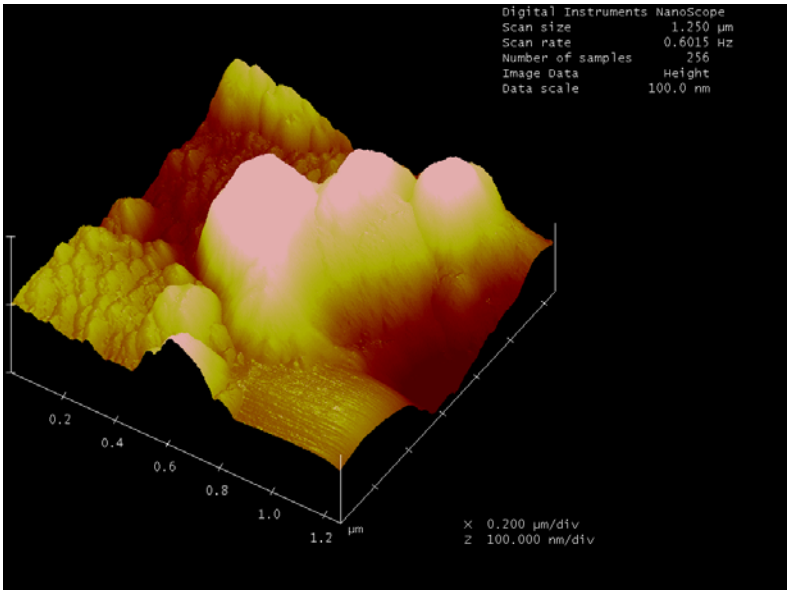

Figure 6. AFM image of hybrid-sized E-glass fiber.

3.2 Handling Friction

The initial role of the fiber-sizing package is to protect the fibers during handling and weaving.

The fiber-sizing package needs to reduce fiber friction during processing, which is accomplished by the film former constituent of the fiber-sizing package.

Increases in handling and processing friction due to the inorganic surface modifying agent were an initial concern and could become a potential issue during manufacture of glass fibers using the hybrid fiber-sizing package.

Ideally, the inorganic fiber surface modifier constituent of the film former package will be deposited primarily to the surface of the glass fibers, through thermodynamic considerations and increased reaction rates, with the film former covering the artificially roughened fiber surfaces.

Once hybrid-sized fibers are incorporated into a composite structure, the film former should diffuse into the matrix resin during infusion and cure, leaving an artificially roughened fiber surface.

No apparent differences between hybrid- and compatible-sized fibers were observed when examined by hand, although FGI reported slight increase in “fuzzing” of hybrid-sized fibers during production.

Only slight increases in force required to pull the roving through the woven fabric were experimentally observed for hybrid-sized fibers in comparison to compatible-sized fibers, as shown in figure 7.

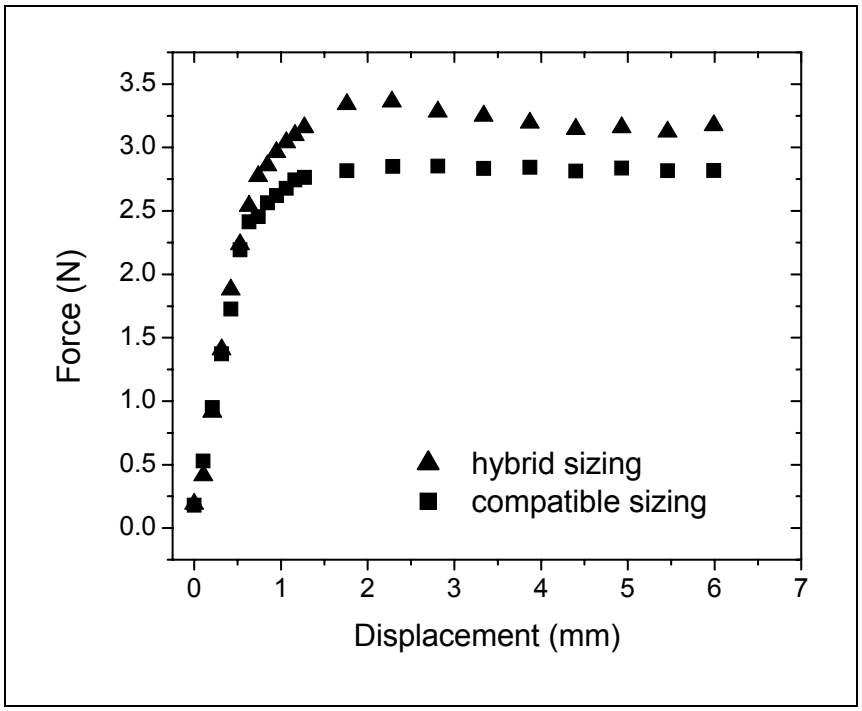

Figure 7. Tensile roving pull-out results from woven E-glass fabric samples.

For the hybrid fiber-sizing package, the film former seemed to be effective in reducing processing friction, which was encouraging from a production standpoint.

Roving Tensile Strengths

Lowering of processing friction is key to reducing fiber breakage during weaving, hence retaining high-tensile strength.

FGI provided complete roving spools that had not undergone any fabric weaving.

The tensile strength of the hybrid-sized fiber rovings decreased from 6.15 to 5.12 kN/m in comparison to the compatible-sized rovings.

As a measure of processing damage incurred during the weaving, the tensile strengths were measured from rovings pulled from both the warp and fill directions of woven fabric for both the hybrid- and compatible-sized fibers. These results are summarized in table 1. After weaving the differences in roving tensile strengths between the hybrid- and compatible-sized fibers were insignificant.

Final conclusions indicate that the effect of the inorganic surface-modifying agent toward increased damage of the glass fibers during processing was minimal.

Table 1. E-glass roving tensile strength summary.

Fiber Sizing	Roving Tensile Strength (kN/m)	Fabric Warp Strength (kN/m)	Fabric Fill Strength (kN/m)
Hybrid	5.12 ± 0.47	2.36 ± 0.27	2.39 ± 0.33
Compatible	6.15 ± 0.47	2.30 ± 0.39	2.13 ± 0.39

3.3 Composite Mechanical Properties

3.3.1 Interfacial Shear Strength (IFSS)

The primary goal of this research project was to increase impact energy resistance of fiber-reinforced composite structures without sacrificing structural performance.

Representative quasi-static force-vs.-displacement curves for composite rods sized with compatible and hybrid fiber sizings using a 3-point bending configuration are shown in figure 8.

Load to break values were slightly higher for the hybrid-sized fiber composite rods.

Calculations of IFSS revealed slightly higher values for the hybrid-sized fibers in comparison to the compatible-sized fibers, particularly at shorter *s*:*d* ratios. Results are summarized in table 2.

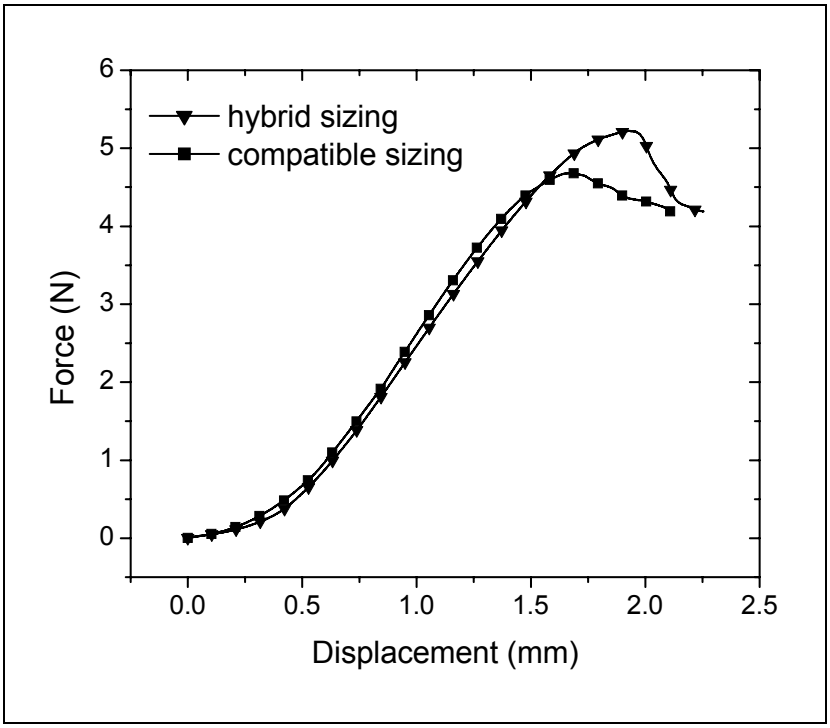

Figure 8. Representative force-vs.-displacement curves for composite rod samples during quasi-static 3-point bend loading.

Table 2. Summary of IFSS for composite rods.

Fiber Sizing	IFSS *s*:*d* = 3:1 (MPa)	IFSS *s*:*d* = 5:1 (MPa)
Hybrid	49.9 ± 6.1	41.7 ± 2.7
Compatible	40.3 ± 0.9	39.8 ± 4.7

3.3.2 Composite Flexural and Tensile Strengths

The quasi-static mechanical results from flexural and tensile testing of composites with hybrid- and compatible-sized E-glass fiber reinforcement are summarized in table 3. S-2 Glass composite samples were also made and tested for comparative purposes.

Table 3. Maximum fiber flexural stress (σ_{max}) and ultimate tensile strengths (F^{tu}) for composite panels reinforced with E-glass fibers treated with hybrid sizing, E-glass fibers treated with epoxy compatible sizing, and S-2 Glass fibers for comparative purposes.

Fiber	σ_{max} *L*:*d* = 10 (MPa)	σ_{max} *L*:*d* = 16 (MPa)	F^{tu} (MPa)
E/hybrid	366 ± 28	411 ± 16	368 ± 14
E/compatible	419 ± 28	506 ± 17	348 ± 16
S-2 Glass	519 ± 25	506 ± 45	546 ± 26

Maximum fiber flexural stress (σ_{max}) at *L*:*d* ratios of 10:1 was lower for the hybrid fiber-sized composites when compared to the compatible fiber-sized composites, 366 vs. 419 MPa, respectively, which is a difference of small significance. σ_{max} measured for the S-2 Glass fiber-reinforced composite were statistically greater at 519 MPa, which is not unexpected as the tensile strength of S-2 Glass (4.59 GPa) is much greater than the tensile strength of E-glass (3.52 GPa) (*56*).

As *L*:*d* ratio was increased to 16:1, σ_{max} increased for the hybrid- and compatible-sized E-glass fiber-reinforced composites. σ_{max} for the compatible-sized E-glass reinforced composite equals the mechanical response of the S-2 Glass reinforced composite.

The ultimate tensile strengths (F^{tu}) measured for the composite samples increased slightly for the hybrid fiber sizing in comparison to the compatible fiber sizing, 368 vs. 348 MPa, respectively, which is a difference of small significance. F^{tu} values recorded for the S-2 Glass reinforced composite were statistically greater at 546 MPa.

The flexural and tensile strength results were as predicted, with the possible exception of the flexural results obtained for the compatible-sized E-glass reinforced composite at *L*:*d* ratio equal to 16:1. The results for this sample seem high, as the mechanical response of the S-2 Glass

reinforced composite was equaled during this loading condition. The coupons for this test set were examined revealing no anomalies in void content, thickness, fiber volume fraction, etc.

With the exception of the previously noted compatible fiber-sized sample, the flexural and tensile strengths of the compatible- and hybrid-sized fiber-reinforced composites were similar.

3.4 Drop Tower Impact Testing

3.4.1 Composite Rods/3-Point Bend

The drop tower impact results for the composite rods in a 3-point bending configuration are illustrated in figure 9 and summarized in table 4.

Hybrid fiber-sized glass-reinforced composite rods achieved statistically similar force to break levels in comparison to the compatible sized rods, 7.2 vs. 6.7 kN, respectively.

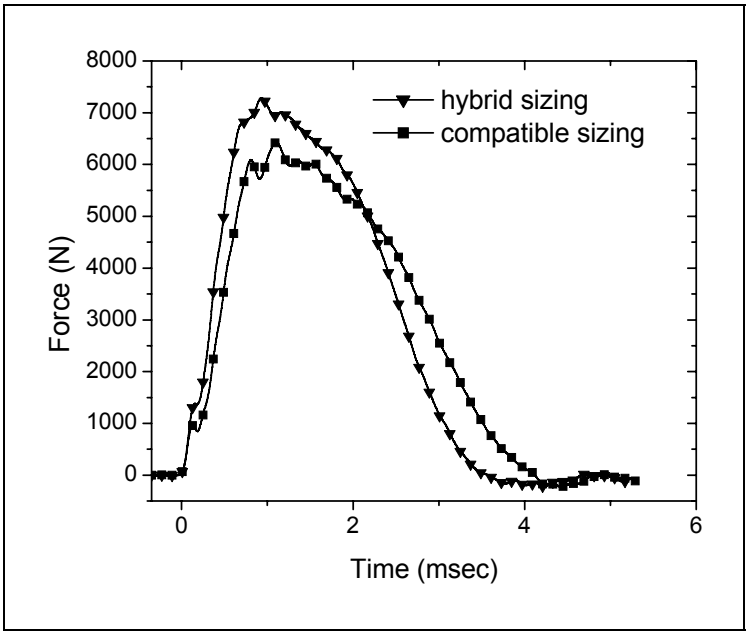

Figure 9. Representative force-vs.-time curves for composite rod samples during 3-point bend impact testing. *s*:*d* ratio = 3:1, E_{impact} = 14.7 J.

Table 4. Summary of drop-tower impact tests for composite rods: *s*:*d* ratio = 3:1, E_{impact} = 14.7 J, V_{impact} = 3.4 m/s.

Fiber Sizing	Maximum Force (kN)	Energy to Maximum Force (J)	Total Energy (J)
Hybrid	7.2 ± 0.4	10.6 ± 1.7	7.9 ± 0.5
Compatible	6.7 ± 0.2	10.6 ± 1.1	8.2 ± 0.5

3.4.2 Flat-Panel Composite Plates

Flat-panel composite plates were tested with E-glass woven fabric with fibers treated with compatible, incompatible, mixed, and hybrid sizings. S-2 Glass reinforced composite panels were also tested for comparative purposes.

The representative force-vs.-time curves for flat E-glass composite panels treated with compatible sizing during impact testing are shown in figure 10. Three different impact energies were tested, referred to as low (E_{impact} = 37 J), medium (E_{impact} = 80 J), and high (E_{impact} = 124 J). At the high impact energy, significant fiber breakage occurs, which resulted in a sharp drop in the load response immediately following the peak maximum.

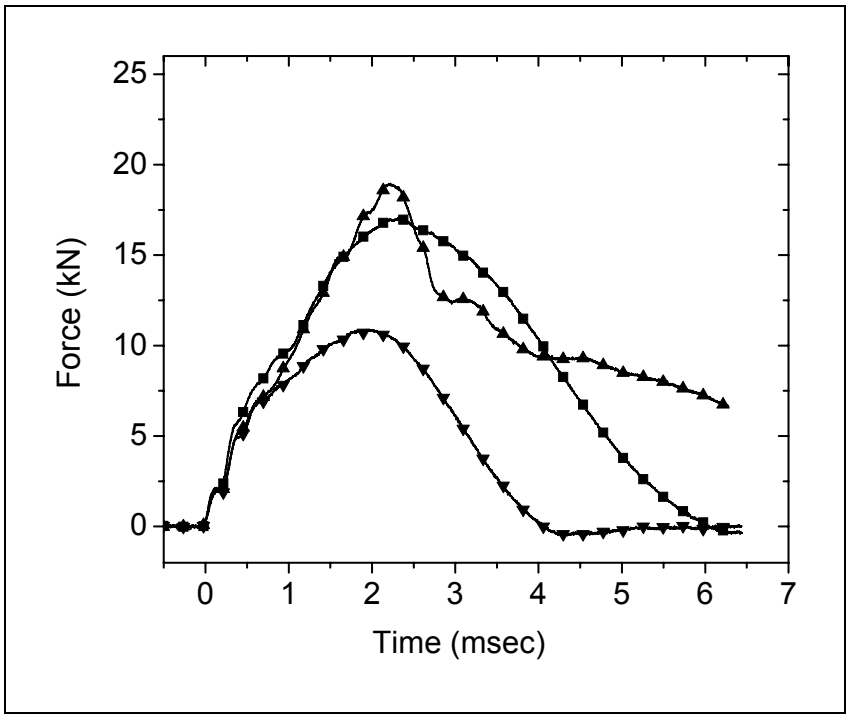

Figure 10. Representative force-vs.-time curves for flat E-glass composite panel treated with compatible sizing during impact testing. (▼) E_{impact} = 37 J, (■) E_{impact} = 80 J, (▲) E_{impact} = 124 J, V_{impact} = 4.5 m/s.

The representative force-vs.-time curves for flat E-glass composite panels treated with incompatible sizing during impact testing are shown in figure 11. The impact response of this sample was similar at low and medium impact energies to the composite panels reinforced with compatible-sized fibers. However, the impact response of the incompatible sizing was remarkably different at high-impact energies, with a gradual rolling over of the force-vs.-time curve. The composite panels reinforced with incompatible-sized fibers displayed a much larger damage area than the composite panels reinforced with compatible-sized fibers at all impact energy levels.

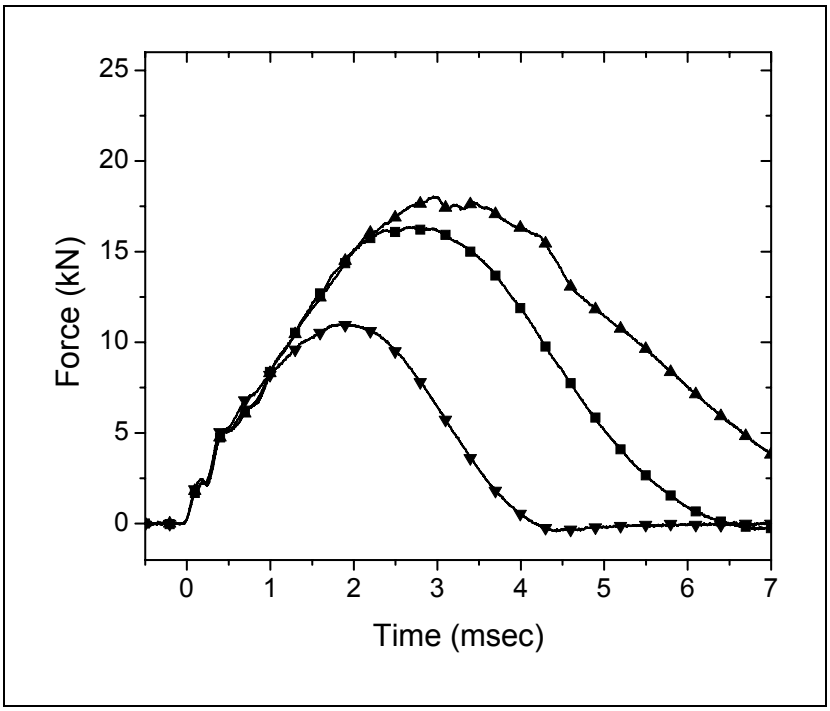

Figure 11. Representative force-vs.-time curves for flat E-glass composite panel treated with incompatible sizing during impact testing. (▼) E_{impact} = 37 J, (■) E_{impact} = 80 J, (▲) E_{impact} = 124 J, V_{impact} = 4.5 m/s.

The representative force-vs.-time curves for flat E-glass composite panels treated with mixed sizing during impact testing are shown in figure 12. These results were interesting in that the impact response curves appear to be very similar to those of the compatible fiber sizing at all impact energies.

The representative force-vs.-time curves for flat E-glass composite panels treated with the hybrid sizing during impact testing are shown in figure 13. The impact response curves were very similar to those of the incompatible fiber sizing. However, the peak load achieved during the high-energy impact was much greater.

The representative force-vs.-time curves for flat S-2 Glass composite panels during impact testing are shown in figure 14. The impact response curves appear to be very similar to those of the E-glass panel treated with compatible fiber sizing. However, the peak load achieved during the high-energy impact is much greater.

The impact response superposition of the composite panels with E-glass fibers treated with hybrid, compatible, mixed, and incompatible fiber sizings at high-impact energies is shown in figure 15. S-2 Glass reinforced composite panel impact response is also shown. For the E-glass

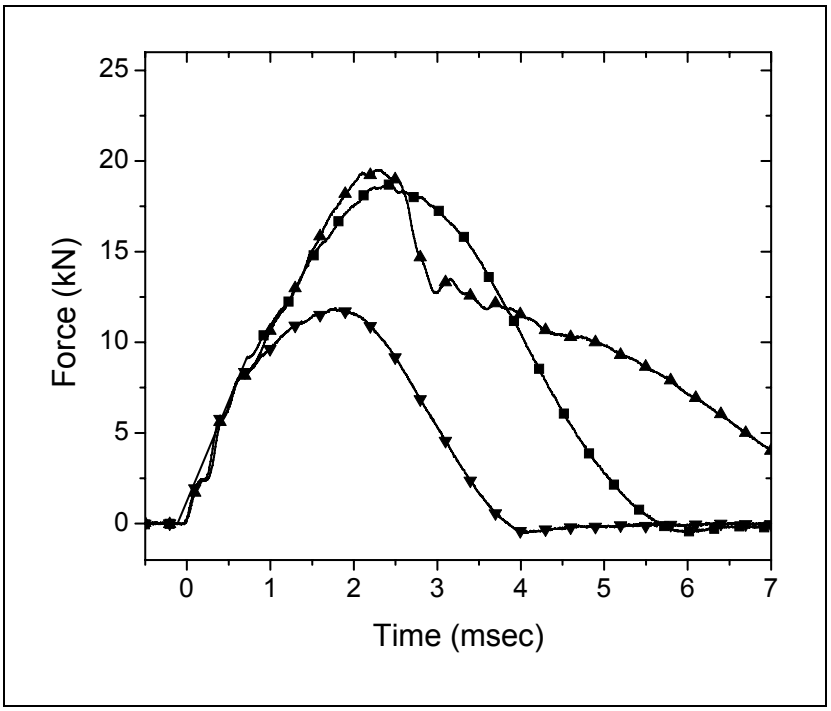

Figure 12. Representative force-vs.-time curves for flat E-glass composite panel treated with mixed sizing during impact testing. (▼) E_{impact} = 37 J, (■) E_{impact} = 80 J, (▲) E_{impact} = 124 J, V_{impact} = 4.5 m/s.

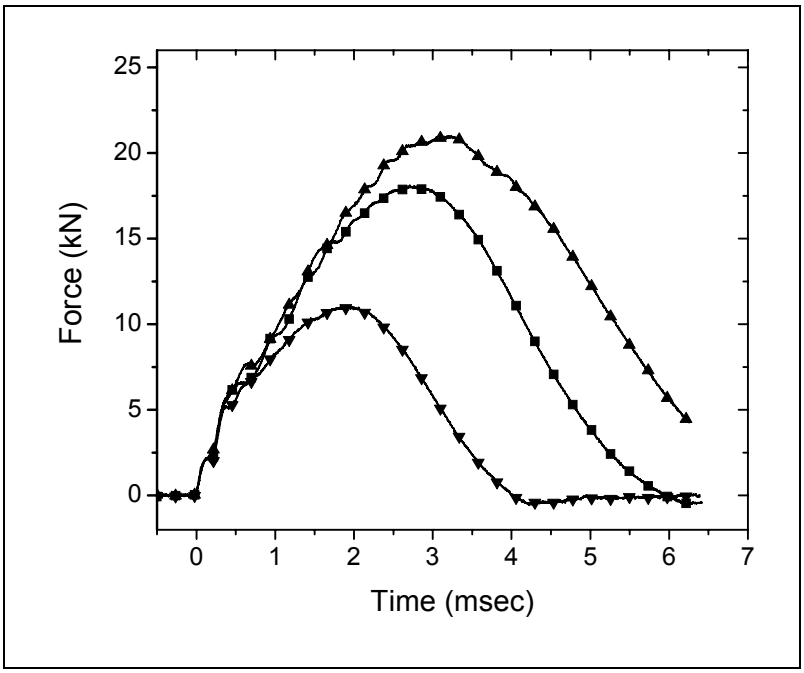

Figure 13. Representative force-vs.-time curves for flat E-glass composite panel treated with hybrid sizing during impact testing. (▼) E_{impact} = 37 J, (■) E_{impact} = 80 J, (▲) E_{impact} = 124 J, V_{impact} = 4.5 m/s.

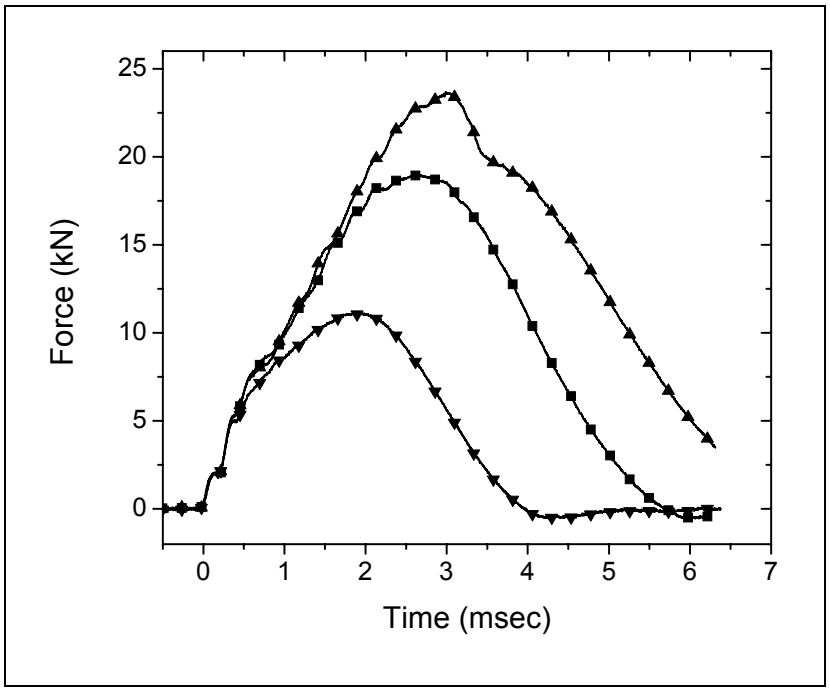

Figure 14. Representative force-vs.-time curves for flat S-2 Glass composite panel treated with epoxy compatible sizing during impact testing. (▼) E_{impact} = 37 J, (■) E_{impact} = 80 J, (▲) E_{impact} = 124 J, V_{impact} = 4.5 m/s.

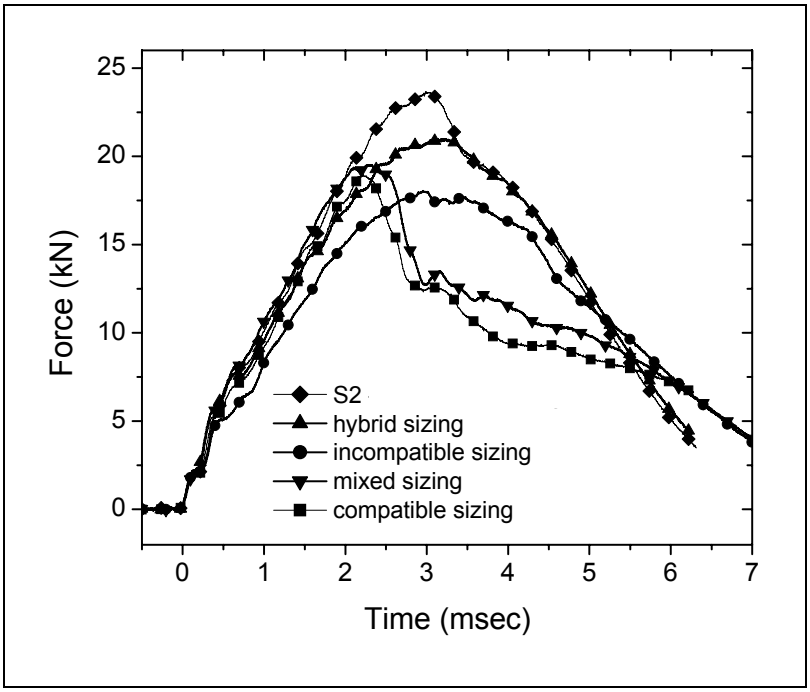

Figure 15. Comparison of composite panel impact response for E-glass fibers treated with hybrid, compatible, mixed, and incompatible fiber sizings. S-2 Glass is also shown. E_{impact} = 124 J, V_{impact} = 4.5 m/s.

composites, the impact load response of the compatible and mixed fiber sizing was similar for times t < 6.5 ms. The incompatible and hybrid sizing response was similar, although the hybrid fiber sizing achieved a greater peak load. The compatible E-glass and S-2 Glass composite impact loading curves look similar with the S-2 response simply shifted to higher values of both maximum force and time. An interesting observation is evident when comparing the impact response of the mixed and incompatible fiber sizings at longer impact times, t > 6.5 ms, as shown in figure 16. Less fiber breakage, seen as the sharp drop in the force-vs.-time plots after the peak force has been achieved, may have been expected based upon the viscoelastic hypothesis outlined in the introduction. This expectation was not apparent at shorter times during the impact event. However, at the longer times, the incompatible and mixed load-vs.-time plots overlay each other. These were the only two sizing combinations with prolonged impact response times.

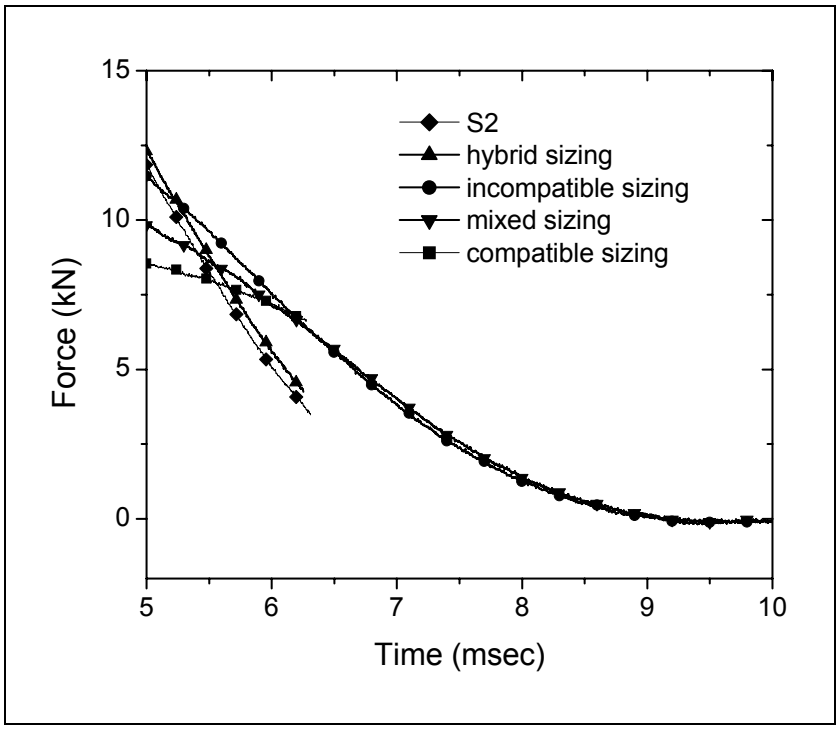

Figure 16. Comparison of composite panel impact response for E-glass fibers treated with hybrid, compatible, mixed, and incompatible fiber sizings. S-2 Glass is also shown. Expanded view of t > 5 ms showing identical force response of mixed and incompatible fiber sizings. E_{impact} = 124 J, V_{impact} = 4.5 m/s.

The plots of impact damage area-vs.-impact energy for the composite panels tested are shown in figure 17. For the compatible and mixed fiber sizings, the damage areas occurred during impact were relatively low. For the incompatible sizing, the impact areas were relatively large at all impact energies. The behavior of the composite containing fibers with the hybrid sizing appeared to shift from compatible to incompatible damage area response as the impact energy

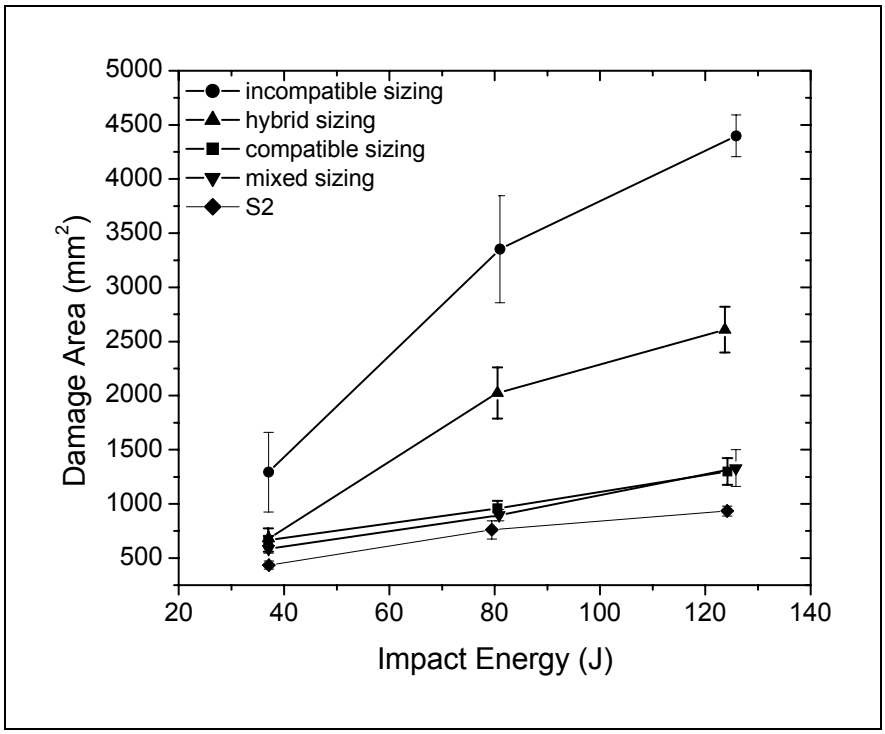

Figure 17. Damage area-vs.-impact energy plots for composite panels with E-glass fibers treated with hybrid, compatible, mixed, and incompatible fiber sizings. S-2 Glass is also shown. V_{impact} = 4.5 m/s.

was increased. At low impact energies, the damage area for the hybrid-sized composite was, within error, identical to the compatible sizing. The hybrid-sized composite exhibits larger damage areas similar to those observed for the incompatible sizing at higher impact energies. The hybrid fiber sizing appears to successfully shift between compatible and incompatible impact response as impact energy is increased, where as the mixed fiber sizing does not. Thus, the viscoelastic response of the fiber-matrix interphase appears to be coupled to the inorganic constituent added to the hybrid fiber sizing. A complete summary of the impact results is given in table 5.

3.4.3 CAI

The CAI results are summarized in table 6. Previously reported literature data state that impact performance and damage tolerance of glass fiber-reinforced composites are profoundly influenced by the silane-coupling agent used to treat the fibers (*17*). As impact resistance is increased by means of an incompatible silane-coupling agent, the structural performance of the composite decreases (*21*). The decrease in structural performance and damage tolerance brought

Table 5. Summary of drop-tower impact testing results for composite panels with E-glass fibers treated with ARL sizing, E-glass fibers treated with FGI standard epoxy compatible sizing, and S-2 Glass fibers treated with epoxy compatible sizing.

Fiber Sizing	Impact Energy (J)	Maximum Force (kN)	Energy to Maximum Force (J)	Total Energy (J)	Damage Area (mm^2)
Hybrid	37.1 ± 0.1	11.0 ± 0.1	36.6 ± 0.2	23.0 ± 0.1	680 ± 20
Compatible	37.0 ± 0.1	10.9 ± 0.2	36.6 ± 0.1	23.4 ± 0.5	670 ± 110
Mixed	37.0 ± 0.1	11.8 ± 0.1	36.8 ± 0.1	19.2 ± 0.1	590 ± 40
Incompatible	37.1 ± 0.1	11.0 ± 0.1	36.6 ± 0.2	20.5 ± 0.4	1290 ± 370
S-2	37.1 ± 0.1	11.2 ± 0.1	36.6 ± 0.4	23.2 ± 0.5	430 ± 40
Hybrid	80.5 ± 0.3	18.1 ± 0.1	78.8 ± 2.3	45.1 ± 1.0	2020 ± 240
Compatible	80.5 ± 0.3	17.3 ± 0.3	73.2 ± 4.9	51.2 ± 1.4	960 ± 70
Mixed	80.9 ± 0.4	18.6 ± 0.1	77.5 ± 4.3	45.9 ± 2.5	900 ± 50
Incompatible	81.0 ± 0.2	16.1 ± 0.2	77.3 ± 1.0	52.2 ± 0.1	3350 ± 500
S-2	79.5 ± 0.3	18.9 ± 0.1	78.7 ± 0.4	40.9 ± 1.2	760 ± 80
Hybrid	123.7 ± 1.0	20.9 ± 0.8	110.5 ± 7.8	89.6 ± 4.1	2610 ± 210
Compatible	124.2 ± 1.3	18.8 ± 1.6	80.4 ± 12.7	123.6 ± 3.1	1300 ± 120
Mixed	125.8 ± 0.4	19.7 ± 0.9	87.7 ± 9.8	105.1 ± 2.6	1330 ± 170
Incompatible	125.8 ± 0.3	17.8 ± 0.4	102.4 ± 9.6	98.9 ± 2.5	4400 ± 190
S-2	124.2 ± 0.2	23.5 ± 0.3	116.1 ± 3.2	81.8 ± 4.2	930 ± 40

about by the use of incompatible silane coupling agents is readily evident in CAI testing. Our results show an approximate 45% decrease in CAI strength of the composite when comparing an incompatible fiber sizing to a compatible sizing. These results were as expected. However, using the hybrid sizing formulation, the CAI strengths of the composite remain comparable to the compatible sizing results. The CAI strength results for the mixed fiber sizing and S-2 composite results are also shown in table 6.□ □

Table 6. Summary of compression after impact testing results for composite panels with E-glass fibers treated with ARL sizing, E-glass fibers treated with FGI standard epoxy compatible sizing, and S-2 Glass fibers for comparative purposes.

Fiber Sizing	Impact Energy (J)	Compressive Strength (MPa)
Hybrid	42.6 ± 0.3	134.4 ± 7.4
Compatible	42.8 ± 0.1	146.0 ± 7.7
Mixed	42.5 ± 0.5	160.6 ± 2.1
Incompatible	42.7 ± 0.2	80.5 ± 6.8
S-2	42.8 ± 0.1	173.8 ± 4.3

□

3.4.4 Composite Layering

The drop tower impact testing results obtained from using alternative fabric lay-ups in the processing of the final composite panels are illustrated in figure 18 and summarized in table 7. Simply stated, the glass-reinforced composite panels contain glass fibers treated with various combinations of compatible and hybrid fiber sizings within the same panel by altering the lay-up order. Other researchers have predicted that increased impact damage resistance could be obtained by stacking the impact side of the composite with brittle layers and the backside with flexible layers (*24*). This type of stacking sequence is theorized to maximize the energy dissipation of the composite by matching the optimal compressive or tensile failure mode with the correct timing and location during the impact event. Our research validated this theory. A pronounced increase in impact resistance was obtained for E-glass fibers treated with compatible sizing for the top half of the panel (impact side) and hybrid sizing for the bottom half of the panel, referred to as "compatible-hybrid (4)" in figure 18 and table 7. The increase in drop tower impact performance was substantial enough for this combination of fiber sizing lay-ups to actually equal the performance of S-2 Glass-reinforced composite in terms of energy to maximum force.

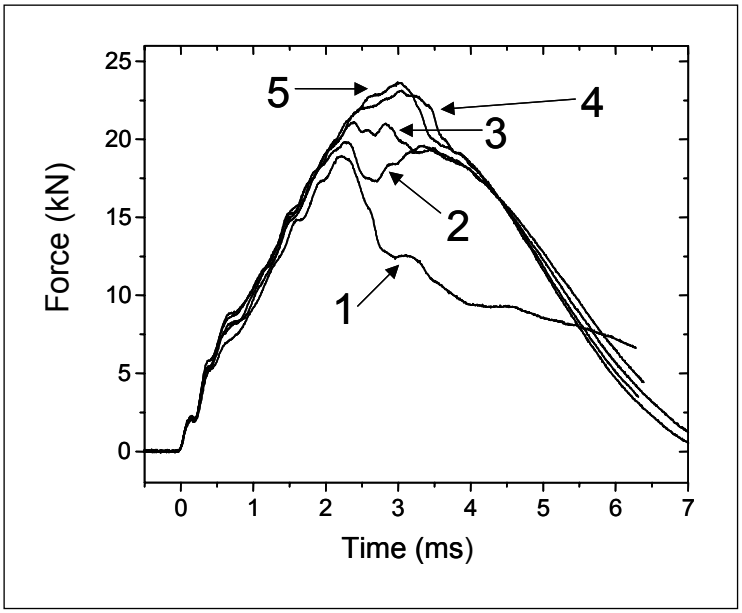

Figure 18. Comparison of composite panel impact response for (1) E-glass fibers treated with epoxy compatible sizing, (2) E-glass fibers treated with compatible sizing in the warp fabric direction and hybrid sizing in the fill fabric direction – 0° fabric lay-up, (3) E-glass fibers treated with compatible sizing in the warp fabric direction and hybrid sizing in the fill fabric direction – 0/90° fabric lay-up, (4) E-glass fibers treated with compatible sizing for the top half of the panel (impact side) and hybrid sizing for the bottom half of the panel, and (5) S-2 Glass fibers for comparative purposes. E_{impact} = 124 J, V_{impact} = 4.5 m/s.

Table 7. Summary of composite panel impact response for (1) E-glass fibers treated with epoxy compatible sizing, (2) E-glass fibers treated with compatible sizing in the warp fabric direction and hybrid sizing in the fill fabric direction – 0° fabric lay-up, (3) E-glass fibers treated with compatible sizing in the warp fabric direction and hybrid sizing in the fill fabric direction – 0/90° fabric lay-up, (4) E-glass fibers treated with compatible sizing for the top half of the panel (impact side) and hybrid sizing for the bottom half of the panel, and (5) S-2 Glass fibers treated with epoxy compatible sizing. E_{impact} = 124 J, V_{impact} = 4.5 m/s.

Fiber Sizing	Maximum Force (kN)	Energy to Maximum Force (J)	Total Energy (J)	Damage Area (mm^2)
Compatible (1)	18.8 ± 1.7	80.4 ± 12.7	123.6 ± 3.1	1300 ± 120
Compatible-hybrid (2)	19.4 ± 1.0	97.7 ± 12.5	90.2 ± 5.1	1380 ± 100
Compatible-hybrid (3)	21.4 ± 0.4	101.0 ± 7.8	82.8 ± 2.5	1660 ± 300
Compatible-hybrid (4)	23.1 ± 0.8	119.8 ± 1.8	80.5 ± 5.1	3150 ± 430
S-2 (5)	23.5 ± 0.3	116.1 ± 3.2	81.8 ± 4.2	930 ± 40

3.4.5 Drop-Tower Impact to Ballistic Correlations

The influence of the fiber-sizing package used on ballistic performance was also examined. A compressed air gas gun was used to strike the composite panels with small-caliber fragment simulator projectiles (FSPs). Energy absorbed to maximum force and total energy absorbed from the drop tower impact tester are plotted with respect to V_{50} results in figure 19 and figure 20, respectively. Some clear qualitative trends between the drop-tower test results and ballistic results are readily apparent. As the energy to maximum load increased, the V_{50} also increased. This result seems intuitive, as the composite requires a greater input of impact energy before undergoing damage. The total energy absorbed was correlated to the ballistic results through a reciprocal relationship. For example, the high reactivity and strong levels of adhesion between the fiber and matrix for the compatible fiber-sizing resulted in significant fiber breakage during an impact event. Fiber breakage is a poor energy absorbing mechanism and leads to a low V_{50}. During the drop tower testing, the impacter struck the composite panel and no upward rebound was observed. Hence, the panel absorbed all of the incoming kinetic impact energy. As the impact/ballistic resistance of the composite panels is increased, the drop tower impacter will begin to rebound after the initial strike, therefore less total energy is absorbed.

V_{50} ranking for E-glass reinforced composite panels followed the trend, compatible < mixed < incompatible, as expected.

Hybrid fiber-sizing V_{50} is improved in comparison to the incompatible sizing, while maintaining structural performance of the compatible sizing.

E-glass reinforced composite compatible-hybrid (4) actually matches ballistic performance of S-2 reinforced composite. The V_{50} value reported for this particular sample is not accurate in that penetration velocities could not be achieved due to the gas gun set-up during this day. Actual V_{50} results should be somewhat greater.

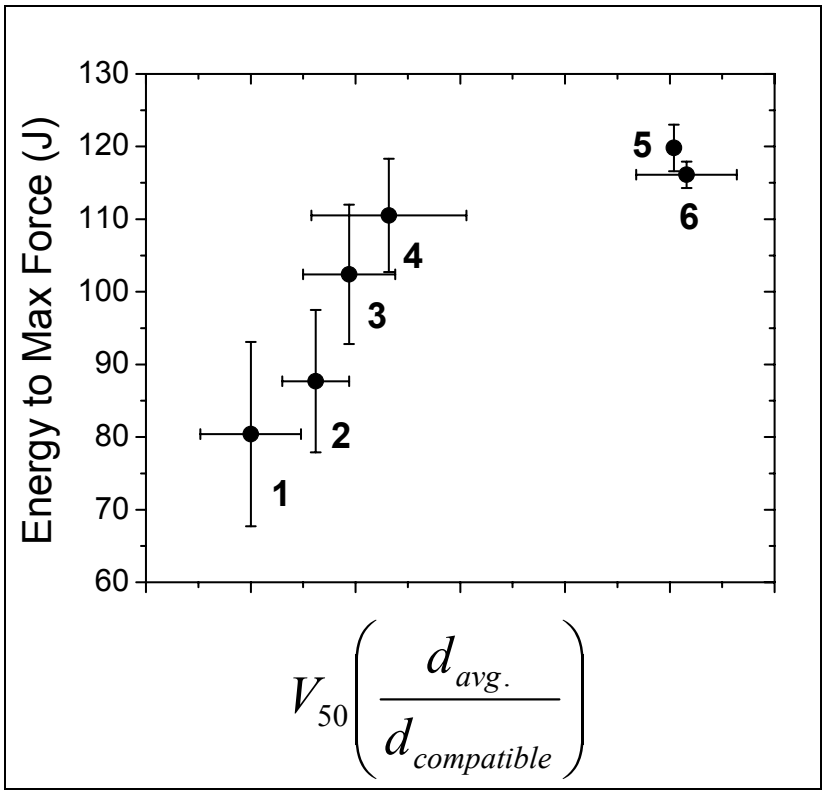

Figure 19. Plot of energy to maximum force absorbed via drop tower impact testing in comparison to V_{50} results obtained with small-caliber FSP. (1) E-glass/compatible sizing, (2) E-glass/mixed sizing, (3) E-glass/incompatible sizing, (4) E-glass/hybrid sizing, (5) E-glass fibers treated with compatible sizing for the top half of the panel (impact side) and hybrid sizing for the bottom half of the panel (no penetration was obtained for this sample), and (6) S-2 Glass.

With proper fiber sizings and composite lay-up stacking sequences, the V_{50} performance of E-glass reinforced composite panels was increased to the V_{50} performance levels achieved using the S-2 Glass reinforcement.

3.5 Moisture Uptake Results

Moisture uptake results at 70 °C (158 °F) for compatible- and hybrid-sized E-glass panels, S-2, and neat epoxy are shown in figure 21. All moisture uptake percentages for the composite samples have been normalized to the matrix mass.

Neat epoxy exhibited nearly Fickian moisture uptake diffusion as expected (*57*).

E-glass reinforced composite samples continue to gain mass after the neat epoxy has reached equilibrium, indicative of microcracking and voiding near the fiber-matrix interphase.

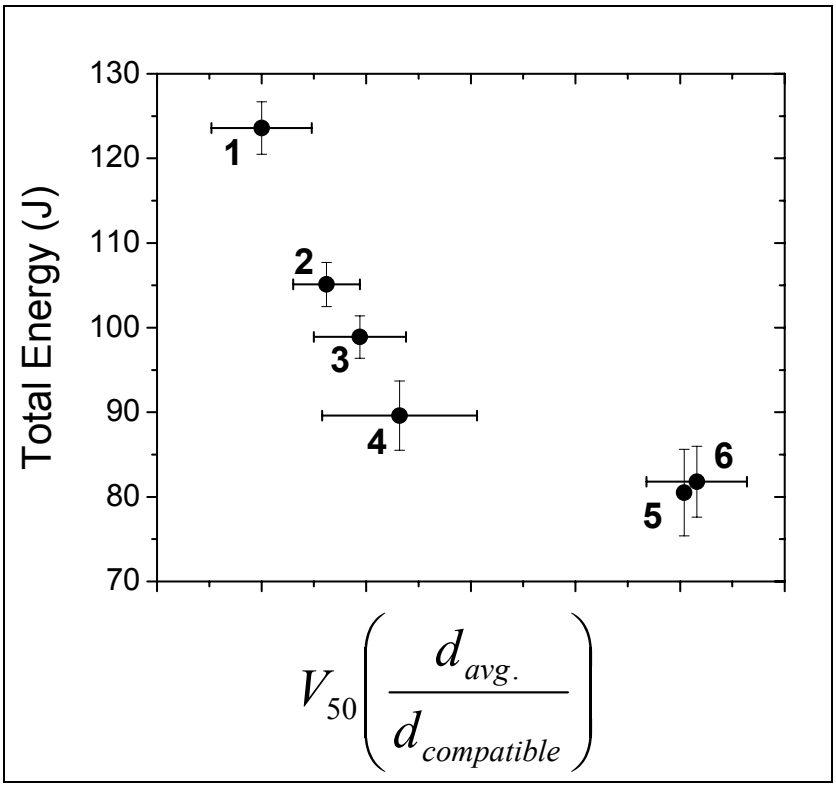

Figure 20. Plot of energy to maximum force absorbed via drop tower impact testing in comparison to V_{50} results obtained with small-caliber FSP. (1) E-glass/compatible sizing, (2) E-glass/mixed sizing, (3) E-glass/incompatible sizing, (4) E-glass/hybrid sizing, (5) E-glass fibers treated with compatible sizing for the top half of the panel (impact side) and hybrid sizing for the bottom half of the panel (no penetration was obtained for this sample), and (6) S-2 Glass.

The S-2 Glass reinforced composite absorbed less water than the E-glass reinforced composites.

Compatible- and hybrid-sized E-glass composites follow similar trends, unlike S-2, probably due to increased fiber corrosion in E-glass when compared to S-2, because more metal hydroxides are present in E-glass.

Compatible and hybrid fiber sizings were still discernable in the drop-tower test after 30 days of exposure as seen in figure 22. The impact performance of S-2 Glass reinforced composite was less affected by moisture exposure. The results are summarized in table 8.

The structural response of composite rods treated with the hybrid fiber sizing after 30 days of moisture exposure at 70 °C was similar to those with the compatible fiber sizing, as summarized in table 9.

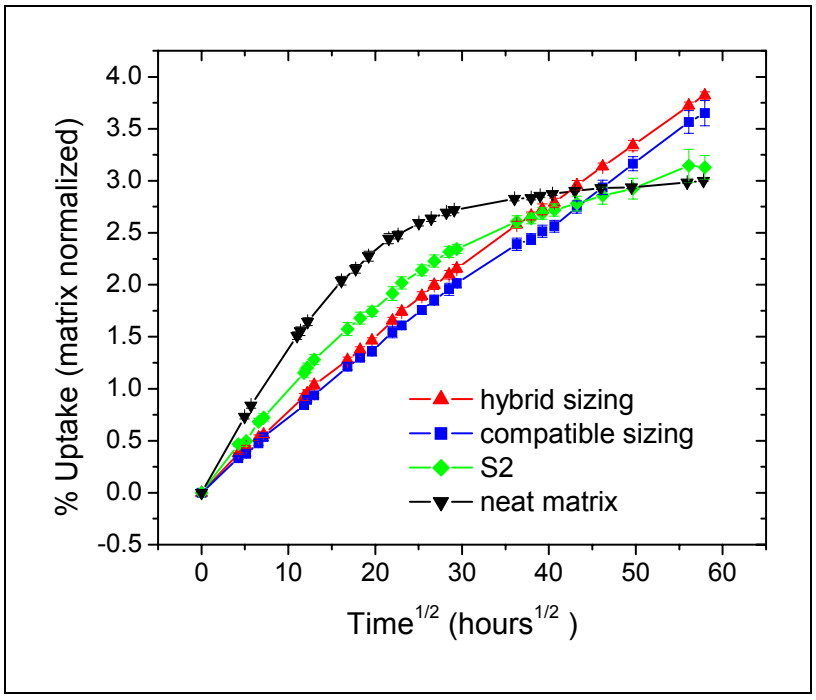

Figure 21. Moisture uptake results for exposure at 70 °C.

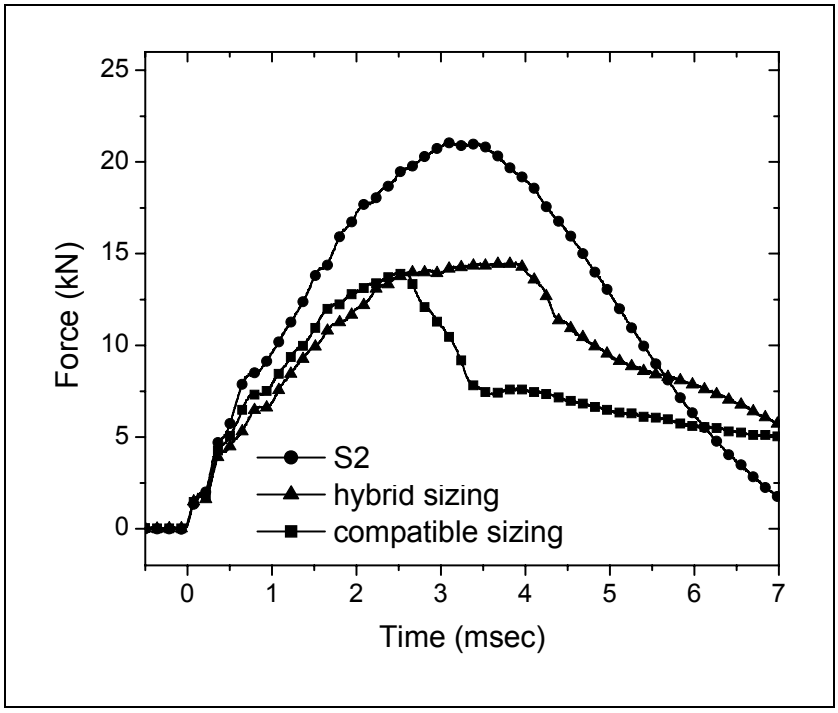

Figure 22. Comparison of composite panel impact response for E-glass fibers treated with epoxy compatible sizing, E-glass fibers treated with hybrid sizing, and S-2 Glass fibers after submersion in water at 70 °C for 30 days. E_{impact} = 124 J, V_{impact} = 4.5 m/s.

Table 8. Summary of composite panel impact response for E-glass fibers treated with epoxy compatible sizing, E-glass fibers treated with hybrid sizing, and S-2 Glass fibers after submersion in water at 70 °C for 30 days. E_{impact} = 124 J, V_{impact} = 4.5 m/s.

Fiber Sizing	Maximum Force (kN)	Energy to Maximum Force (J)	Total Energy (J)	Damage Area (mm^2)
E/hybrid	14.8 ± 0.4	105.5 ± 11.2	109.8 ± 0.8	3460 ± 280
E/compatible	14.1 ± 0.6	82.5 ± 3.9	119.3 ± 2.1	1660 ± 450
S-2	21.0 ± 0.2	117.6 ± 4.3	82.6 ± 0.2	2680 ± 530

Table 9. Summary of wet IFSS for composite rods.

Fiber Sizing	IFSS *s*:*d* = 3:1 (MPa)	IFSS *s*:*d* = 5:1 (MPa)
Hybrid	45.4 ± 3.0	41.1 ± 2.3
Compatible	43.9 ± 3.4	41.1 ± 3.7

4. Conclusions

The achievement of excellent structural properties with concurrent superior impact energy absorption/ballistic resistance in glass fiber-reinforced composites has traditionally been unobtainable. The chemistry of the fiber-matrix interphase has been determined to be the key driving force in determining if good structural compatible fiber sizing or good ballistic incompatible fiber sizing performance from the composite material was to be realized, with one aspect of performance being traded for the other. Through a careful understanding of the failure mechanisms during fiber-matrix push-out, associated energy absorption relationships, and viscoelastic properties of the fiber-matrix interphase a novel fiber sizing was developed that "triggers" between structural response at low impact energies and ballistic response at high impact energies. Furthermore, increasing the surface roughness of the fibers enhanced the ballistic energy absorption capabilities of the composites tested. This new type of hybrid fiber sizing was successfully manufactured at a commercial production facility with minimal difficulties and incurring no added cost in comparison to a standard structural fiber sizing. The new hybrid fiber sizing shows no significant differences when compared to the assets of a structural fiber sizing, which are low moisture absorption and high compression after impact strengths. The new hybrid fiber sizing also exceeds the impact and ballistic performance of a traditional incompatible ballistic fiber sizing.

5. References

1. Ishida, H.; Koenig, J. L. Fourier-Transform Infrared Spectroscopic Study of Structure of Silane Coupling Agent on E-Glass Fiber. *Journal of Colloid Interface Science* **1978**, *64*, 565–576.
2. Drzal, L. T. The Role of the Fiber-Matrix Interphase on Composite Properties. *Vacuum* **1990**, *41*, 1615–1618.
3. Fink, B. K.; McCullough, R. L. Interphase Research Issues. *Composites Part A* **1999**, *30*, 1–2.
4. Wang, D.; Jones, F. R. Surface Analytical Study of the Interaction Between γ-Amino Propyl Triethoxysilane and E-Glass Surface. *Journal of Materials Science* **1993**, 2481–2487.
5. Horner, M. R.; Boerio, F. J.; Clearfield, H. M. An XPS Investigation of the Adsorption of Aminosilanes Onto Metal Substrates. In VSP: Netherlands, 1992; pp 241–262. In *Silanes and Other Coupling Agents*; Mittal, K. L., Ed.; in VSP: Netherlands, 1992; pp 241–262.
6. Kim J. K.; Hodzic A. Nanoscale Characterization of Thickness and Properties of Interphase in Polymer Matrix Composites. *Journal of Adhesion* **2003**, *79*, 383–414.
7. Ishida, H.; Koenig, J. L. The Reinforcement Mechanism of Fiber-Glass Reinforced Plastics Under Wet Conditions: A Review. *Polymer Engineering and Science* **1978**, *18*, 128–144.
8. Saidpour, S. H.; Richardson, M. O. W. Glass Fibre Coating for Optimum Mechanical Properties of Vinyl Ester Composites. *Composites Part A* **1997**, *28A*, 971–975.
9. Plueddemann, E. P. *Silane Coupling Agents*; 2nd ed.; New York: Plenum Press, 1990.
10. Park, S. J.; Jin, J. S. Effect of Silane Coupling Agent on Interphase and Performance of Glass Fibers/Unsaturated Polyester Composites. *Journal of Colloid Interface Science* **2001**, *242*, 174–179.
11. Salmon, L.; Thominette, F.; Pays, M. F.; Verdu, J. Hydrolytic Degradation of Model Networks Simulating the Interfacial Layers in Silane-Coupled Epoxy/Glass Composites. *Composites Science and Technology* **1997**, *57*, 1119–1127.
12. Thomason, J. L.; Dwight, D. W. The Use of XPS for Characterization of Glass Fibre Coatings. *Composites Part A* **1999**, *30*, 1401–1413.
13. Larson, B. K.; Drzal, L. T.; Van Antwerp, J. Swelling and Dissolution Rates of Glass Giber Sizings in Matrix Resin Via Micro-Dielectrometry. *Polymer Composites* **1995**, *16*, 415–420.

14. Wu, H. F.; Dwight, D. W.; Huff, N. T. Effects of Silane Coupling Agents on the Interphase and Performance of Glass-Fiber-Reinforced Polymer Composites. *Composites Science and Technology* **1997**, *57*, 975–983.

15. Hsiao, H. M.; Daniel, I. M.; Cordes, R. D. Dynamic Compressive Behavior of Thick Composite Materials. *Experimental Mechanics* **1998**, *38*, 172–180.

16. Barre, S.; Chotard, T.; Benzeggagh, M. L. Comparative Study of Strain Rate Effects on Mechanical Properties of Glass Fibre-Reinforced Thermoset Matrix Composites. *Composites Part A* **1996**, *27*, 1169–1181.

17. Kim, J. K.; Sham, M. L. Impact and Delamination Failure of Woven-Fabric Composites. *Composites Science and Technology* **2000**, *60*, *745–761*.

18. Cantwell, W. J.; Tato, W.; Kausch, H. H. The Influence of a Fiber-Matrix Coupling Agent on the Properties of a Glass Fiber/Polypropylene GMT. *Journal of Thermoplastic Composite Materials* **1992**, *5*, 304–317.

19. Cantwell, W. J.; Morton, J. The Impact Resistance of Composite Materials—A Review. *Composites* **1991**, *22*, 347–362.

20. Peterson, B. L.; Pangborn, R. N.; Pantano, C. G. Static and High Strain Rate Response of a Glass Fiber Reinforced Thermoplastic. *Journal of Composite Materials* **1991**, *25*, 887–906.

21. Hartman, D. R. Ballistic Impact Behavior of High-Strength Glass-Fiber Composites. 41st Annual Conference, Reinforced Plastics/Composites Institute, The Society of the Plastics Industry, Inc., 27–31 January 1986.

22. Kessler, A.; Bledzki, A. Correlation Between Interphase-Relevant Tests and the Impact-Damage Resistance of Glass/Epoxy Laminates With Different Surface Treatments. *Composites Science and Technology* **2000**, *60*, 125–130.

23. Hirai, Y.; Hamada, H.; Kim, J. K. Impact Response of Woven Glass-Fabric Composites – I. Effect of Fibre Surface Treatment. *Composites Science and Technology* **1998**, *58*, 91–104.

24. Kim, J. K.; Sham, M. L.; Sohn, M. S.; Hamada, H. Effect of Hybrid Layers With Different Silane Coupling Agents on Impact Response of Glass Fabric Reinforced Vinylester Matrix Composites. *Polymer* **2001**, *4*, 7455–7460.

25. Lee, I.; Wool, R. P. Polymer Adhesion vs. Substrate Receptor Group Density. *Macromolecules* **2000**, *33*, 2680–2687.

26. Kent, M. S.; Yim, H.; Matheson, A.; Cogdill, C.; Nelson, G.; Reedy, E. D. Use of Self-Assembled Monolayers at Variable Coverage to Control Interface Bonding in a Model Study of Interfacial Fracture: Pure Shear Loading. *Journal of Adhesion* **2001**, *75*, 267–298.

27. Ferry, J. D. *Viscoelastic Properties of Polymers*; 2nd ed.; John Wiley & Sons: New York, 1970.

28. Tanoglu, M.; McKnight, S. H.; Palmese, G. R.; Gillespie, J. W. The Effects of Glass-Fiber Sizings on the Strength and Energy Absorption of the Fiber/Matrix Interphase Under High Loading Rates. *Composites Science and Technology* **2001**, *61* (2), 205–220.

29. Jackson, C. L.; Bauer, B. J.; Nakatani, A. I.; Barnes, J. D. Synthesis of Hybrid Organic-Inorganic Materials From Interpenetrating Polymer Network Chemistry. *Chemistry of Materials* **1996**, *8*, 727–733.

30. Breiner, J. M.; Mark, J. E.; Beaucage, G. Dependence of Silica Particle Sizes on Network Chain Lengths, Silica Contents, and Catalyst Concentrations in In Situ Reinforced Polysiloxane Elastomers. *Journal of Polymer Science: Part B: Polymer Physics* **1999**, *37*, 1421–1427.

31. Huang, Z. H.; Dong, J. H.; Qui, K. Y.; Wei, Y. New Hybrid Materials Incorporating Tetrabutyl Titanate and Tetraethoxysilane With Functional SEBS Elastomer Via the Sol-Gel Process: Synthesis and Characterization. *Journal of Applied Polymer Science* **1997**, *66*, 853–860.

32. Juangvanich, N.; Mauritz, K. A. Polyethersulfone –[Silicon Oxide] Hybrid Materials Via In Situ Sol-Gel Reactions for Tetra-Alkoxysilanes. *Journal of Applied Polymer Science* **1998**, *67*, 1799–1810.

33. Matejka, L.; Plestil, J.; Dusek, K. Structure Evolution in Epoxy-Silica Hybrids: Sol-Gel Process. *Journal of Non-Crystalline Solids* **1998**, *226*, 114–121.

34. Wen, J.; Wilkes, G. L. Organic/Inorganic Hybrid Network Materials by the Sol-Gel Approach. *Chemistry of Materials* **1996**, *8*, 1667–1681.

35. McCarthy, D. W.; Mark, J. E.; Clarson, S. J.; Schaefer, D. W. Synthesis, Structure, and Properties of Hybrid Organic-Inorganic Composites Based on Polysiloxanes. II. Comparisons Between Poly(Methylphenylsiloxane) and Poly(Dimethylsiloxane), and Between Titania and Silica. *Journal of Polymer Science: Part B: Polymer Physics* **1998**, *36*, 1191–1200.

36. Prabakar, S.; Assink, R. A. Hydrolysis and Condensation Kinetics of Two Component Organically Modified Silica Sols. *Journal of Non-Crystalline Solids* **1997**, *211*, 39–48.

37. Krakovsky, I.; Urakawa, H.; Kajiwara, K.; Kohjiya, K. Time Resolved Small Angle X-Ray Scattering of Inorganic-Organic Gel Formation Kinetics. *Journal of Non-Crystalline Solids* **1998**, *231*, 31–40.

38. Li, X.; King, T. Microstructure and Optical Properties of PMMA/Gel Silica Glass Composites. *Journal of Sol-Gel Science and Technology* **1995**, *4*, 75–82.

39. Haas, K. H.; Schwab, S. A.; Rose, K. Functionalized Coating Materials Based on Inorganic-Organic Polymers. *Thin Solid Films* **1999**, *351*, 198–203.

40. Langroudi, A. E.; Mai, C.; Vigier, G.; Vassoille, R. Hydrophobic Hybrid Inorganic-Organic Thin Film Prepared by Sol-Gel Process for Glass Protection and Strengthening Applications. *Journal of Applied Polymer Science* **1997**, *65*, 2387–2393.

41. Chen, J. I.; Chareonsak, R.; Puengripat, V.; Marturunkakul, S. Organic/Inorganic Composite Materials for Coating Applications. *Journal of Applied Polymer Science* **1999**, *74*, 1341–1346.

42. Nikolic, L.; Radonjic, L. Effect of the Silica Sol-Gel Coatings on the Properties of Glass Substrate. *Ceramics International* **1998**, *24*, 547–552.

43. Osborne, J. H.; Blohowiak, K. Y.; Taylor, S. R.; Hunter, C.; Bierwagon, G.; Carlson, B.; Bernard, D.; Donley, M. S. Testing and Evaluation of Nonchromated Coating Systems for Aerospace Applications. *Progress in Organic Coatings* **2001**, *41*, 217–225.

44. Wold, C. R.; Soucek, M. D. Mixed Metal Oxide Inorganic/Organic Coatings. *Journal of Coatings Technology* **1998,** *70*, 43–51.

45. Khobaib, M.; Reynolds, L. B.; Donley, M. S. A Comparative Evaluation of Corrosion Protection of Sol-Gel Based Coatings Systems. *Surface & Coatings Technology* **2001**, *140*, 16–23.

46. Thomason, J. L. The Interface Region in Glass Fibre-Reinforced Epoxy Resin Composites: Sample Preparation, Void Content and Interfacial Strength. *Composites* **1995**, *26*, 467–475.

47. Gorowara, R. L. *Interphase Formation and Environmental Degradation in Glass Fiber/Vinyl Ester Composites*; Ph.D. Thesis, University of Delaware, Center for Composite Materials and Department of Chemical Engineering, 2001.

48. Hsiao, K. T.; Gillespie, J. W.; Advani, S. G.; Fink, B. K. Role of Vacuum Pressure and Port Locations on Flow Front Control for Liquid Composite Molding Processes. *Polymer Composites* **2001**, *22*, 660–667.

49. ASTM D 792-00. Standard Test Methods for Density and Specific Gravity (relative density) of Plastics by Displacement. *Annu. Book ASTM Stand*. **2000**.

50. ASTM D 4475-85. Standard Test Method for Apparent Horizontal Shear Strength of Pultruded Reinforced Plastic Rods by the Short-Beam Method. *Annu. Book ASTM Stand.* **1985**.

51. ASTM D 790-96a. Standard Test Methods for Flexural Properties of Unreinforced and Reinforced Plastics and Electrical Insulating Materials. *Annu. Book ASTM Stand*. **1996**.

52. ASTM D 3039/D 3039M-95a. Standard Test Methods for Tensile Properties of Polymer Matrix Composite Materials. *Annu*. *Book ASTM Stand*. **1995**.

53. Instron Dynatup 930-1, version 1.21

54. ImageJ, version 1.30. National Institute of Health.; W. Rasband.

55. Suppliers of Advance Composite Materials Association, SACMA Recommended Test Method for Compression After Impact Properties of Oriented Fiber-Resin Composites. SRM 2R-94, Arlington, VA, 1994.

56. Katz, H. S.; Milewski, J. *Handbook of Reinforcement for Plastics*; Van Nostrand Reinhold, 1987.

57. Chen, C. H.; Springer, G. S. Moisture Absorption and Desorption of Composite Materials. *Journal of Composite Materials* **1976**, *10*, 2–20.

NO. OF COPIES ORGANIZATION

1 (PDF Only) DEFENSE TECHNICAL INFORMATION CTR
DTIC OCA
8725 JOHN J KINGMAN RD
STE 0944
FT BELVOIR VA 22060-6218

1 COMMANDING GENERAL
US ARMY MATERIEL CMD
AMCRDA TF
5001 EISENHOWER AVE
ALEXANDRIA VA 22333-0001

1 INST FOR ADVNCD TCHNLGY
THE UNIV OF TEXAS
AT AUSTIN
3925 W BRAKER LN STE 400
AUSTIN TX 78759-5316

1 US MILITARY ACADEMY
MATH SCI CTR EXCELLENCE
MADN MATH
THAYER HALL
WEST POINT NY 10996-1786

1 DIRECTOR
US ARMY RESEARCH LAB
AMSRD ARL CS IS R
2800 POWDER MILL RD
ADELPHI MD 20783-1197

3 DIRECTOR
US ARMY RESEARCH LAB
AMSRD ARL CI OK TL
2800 POWDER MILL RD
ADELPHI MD 20783-1197

3 DIRECTOR
US ARMY RESEARCH LAB
AMSRD ARL CS IS T
2800 POWDER MILL RD
ADELPHI MD 20783-1197

NO. OF COPIES ORGANIZATION

ABERDEEN PROVING GROUND

1 DIR USARL
AMSRD ARL CI OK TP (BLDG 4600)

NO. OF COPIES ORGANIZATION

1 DPTY ASST SECY FOR R&T
SARD TT
THE PENTAGON
RM 3EA79
WASHINGTON DC 20301-7100

1 COMMANDER
US ARMY ARDEC
AMSTA AR WET
T SACHAR
BLDG 172
PICATINNY ARSENAL NJ
07806-5000

1 COMMANDER
US ARMY ARDEC
AMSTA AR WEA
J BRESCIA
PICATINNY ARSENAL NJ
07806-5000

1 COMMANDER
US ARMY TACOM
AMSTA SF
WARREN MI 48397-5000

2 COMMANDER
US ARMY AMCOM
AVIATION APPLIED TECH DIR
J SCHUCK
FT EUSTIS VA 23604-5577

3 COMMANDER
US ARMY TACOM
AMSTA JSK
J FLORENCE
AMSTA TR D
D OSTBERG
S HODGES
WARREN MI 48397-5000

2 USA SBCCOM
MATERIAL SCIENCE TEAM
AMSSB RSS
J HERBERT
M SENNETT
KANSAS ST
NATICK MA 01760-5057

NO. OF COPIES ORGANIZATION

1 NAVAL SURFACE WARFARE CTR
TECH LIBRARY CODE 323
17320 DAHLGREN RD
DAHLGREN VA 22448

4 US ARMY RESEARCH OFC
A CROWSON
D STEPP
D KISEROW
J CHANG
PO BOX 12211
RSCH TRIANGLE PARK NC
27709-2211

2 NAVAL SURFACE WARFARE CTR
CARDEROCK DIVISION
R CRANE CODE 2802
C WILLIAMS CODE 6553
3A LEGGETT CIR
BETHESDA MD 20054-5000

2 AFRL
F ABRAMS
J BROWN
BLDG 653
2977 P ST STE 6
WRIGHT PATTERSON AFB OH
45433-7739

1 NASA LANGLEY RSCH CTR
AMSRL VS
W ELBER MS 266
BLDG 653
HAMPTON VA 23681-0001